Wind Conditions for Snow Cornice Formation in a Wind Tunnel

Hongxiang Yu[1,3], Guang Li[2,3], Benjamin Walter[4], Michael Lehning[3,4], Jie Zhang[1], and Ning Huang[1]

[1]College of Civil engineering and Mechanics, Lanzhou University, Lanzhou, 730000, China
[2]College of Atmospheric Science, Lanzhou University, Lanzhou, 730000, China
[3]College of Architecture Civil and Environmental Engineering, Ecole Polytechnique Federal de Lausanne, Lausanne, 1015, Switzerland
[4]WSL Institute for Snow and Avalanche Research SLF, Davos, 7260, Switzerland

Correspondence: Ning Huang (huangn@lzu.edu.cn)

Abstract. Snow cornices growing on the leeward side of mountain ridges are common in alpine and polar regions during snow seasons. These structures may crack and fall, leading to an increase in the avalanche danger. Although cornice formation has been observed in wind tunnel tests and the field, knowledge gaps still exist regarding the formation mechanism. In particular with respect to wind conditions, which favor cornice formation. To characterize the wind effects as the main factor for cornice growth, we carried out ring wind tunnel (RWT) experiments in a cold laboratory under various wind conditions. We quantitatively investigated the growth rate of the cornice in the horizontal and vertical direction, as well as the airborne particle concentration. The results show that cornices only appear under a moderate wind speed range (1-2.03 $\tilde{u}$). The cornice growth rates in length and thickness are mainly determined by the combined effects of mass accumulation and erosion. The lower limit wind speed for cornice growth is approximately equal to the threshold wind speed for transport. The upper limit of wind speed is when the erosion rate is over the pure deposition rate. The length growth rates of cornice reach a maximum for wind speeds approximately 40$\%$ higher than the threshold wind speed. Moreover, a conceptual model for interpreting the cornice accretion mechanism is proposed based on the mass conservation and the results of the RWT experiments. The estimated suitable wind condition for cornice growth and formation are in good agreement with the field observations in Gruvefjellet, Svalbard. This work could be helpful in the snow avalanche prediction works.

NOTATION

Symbol	Definition and units
t	Time [s]
ρ_{i}	Ice density [kg m^{-3}]
ρ_{c}	Cornice density [kg m^{-3}]
ρ_{a}	Air density [kg m^{-3}]
d_{p}	Particle diameter [m]
z	Height above snow surface [m]
p	Depth of field [m]
E	Collection efficiency [%]
A_0	Area of one pixel [m^2]
S_0	Area of window Ω [m^2]
S_c	Cornice area [m^2 s^{-1}]
L	Cornice length [m]
H	Cornice thickness [m]
l_g	Growth rate in length [m s^{-1}]
l_g^f	Growth rate in length the field [m s^{-1}]
h_g	Growth rate in thickness [m s^{-1}]
l_d	Pure deposition rate in length [m s^{-1}]
h_d	Pure deposition rate in thickness [m s^{-1}]
l_e	Erosion rate in length [m s^{-1}]
h_e	Erosion rate in thickness [m s^{-1}]
$\bar{l}_g$	Averaged growth rate in length [m s^{-1}]
$\bar{h}_g$	Averaged growth rate in thickness [m s^{-1}]
$\bar{l}_d$	Averaged pure deposition rate in length [m s^{-1}]
$\bar{h}_d$	Averaged pure deposition rate in thickness [m s^{-1}]
$\bar{l}_e$	Averaged erosion rate in length [m s^{-1}]
$\bar{h}_e$	Averaged erosion rate in thickness [m s^{-1}]
u	Wind speed [m s^{-1}]
u_t	Threshold wind speed [m s^{-1}]
u_f	Field wind speed [m s^{-1}]
u_*	Friction velocity [m s^{-1}]
u_{*t}	Threshold friction velocity [m s^{-1}]
$\tilde{u}$	Non-dimensional wind speed
$\bar{u}$	Daily averaged wind speed [m s^{-1}]

NOTATION

u_p	Particle velocity [m s^{-1}]
K_d	Deposition coefficient [m s^{-1}]
f_l	Horizontal collection coefficient [m s^{-1}]
q_p	Particle mass flux [kg m^{-2} s^{-1}]
ϕ_p	Mass concentration of particles in the air [kg m^{-3}]
Q	Transport rate [kg m^{-1} s^{-1}]
g	Gravitational acceleration [= 9.81 m s^{-2}]
κ	Von Kármán constant [= 0.4]
M_e	Erosion rate of mass [kg m^{-2} s^{-1}]
η_{ae}	Aerodynamic entrainment coefficient [grains N^{-1} s^{-1}]
m_p	One particle mass [kg]

1 Introduction

Snow cornices are leeward-growing masses of snow overhanging and extending horizontally beyond the edge, usually appearing on the ridgeline of steep mountains (Seligman et al., 1936). Some cornices deform, detach, and eventually fall off, which induces cornice fall avalanches or slope erosion, and leads to a redistribution of the snow cover below (Wahl et al., 2009). For example, cornice fall avalanches accounted for 45.2 % of all 423 snow avalanches observed in the Longyearbyen area, central Svalbard, from 2006 to 2009. They triggered slab avalanches and loose snow avalanches as secondary avalanches on the slope below (Eckerstorfer and Christiansen, 2011). Cornice fall avalanches cause potential threats to local infrastructures and human lives.

Although understanding the initial evolution of cornices is a foundation for predicting and treating cornice fall avalanches, only a few studies have paid attention to the initial accretion process, especially to the horizontal extension forming the main part of the snow mass overhanging the edge of a mountain crest. Previous research has observed that cornices grow under moderate wind speeds. However, gaps remain regarding a general rule on suitable wind conditions for cornice growth. Montagnen et al. (1968) measured the moderate wind speed range is between 7 to 15 m s^{-1} (at 0.35 m height) for cornice formation using a hand anemometer. Naito and Kobayashi (1986) measured the suitable wind speed for cornice formation is between 4 m s^{-1} to 8 m s^{-1}, at 1 m above the snow surface in the field and at the center (0.5 m height) in the wind tunnel. McClung and Schaerer (2006) estimated that the threshold wind speed for cornice growth and formation is about 5 to 10 m s^{-1} (at 10 m height) which is the threshold wind speed for loose snow transport, and scouring happens when the wind speed exceeds 25 m s^{-1}. Vogel et al. (2012) determined that cornice accretion occurs during periods with the average wind speed of 12 m s^{-1}, and scour when the wind speed exceeds 30 m s^{-1} (at 2.8 m height). Hancock et al. (2020) used an experienced value of threshold wind speed of 5 m s^{-1} (at 10 m height) as a conservative lower threshold for cornice accretion. However, to our best knowledge, this discrepancy and the conditions under which certain wind speed ranges apply have not been investigated.

Indirect evidence was presented by van Herwijnen and Fierz (2014) that snow cornices only grow under the moderate to strong wind, during or soon after a snowfall. The cornice width from observation is in remarkable agreement with the wind drift index calculated by the snow cover model SNOWPACK (Lehning and Fierz, 2008), which indicates that snow mass transport plays an important role in cornice formation. However, cornices often grow through relatively discrete events in the field (Vogel et al., 2012; van Herwijnen and Fierz, 2014; Naito and Kobayashi, 1986; Hancock et al., 2020), average observations (daily) therefore only incompletely characterize cornice growth conditions. Due to the compromise of these field observations, continuous observations on individual cornice accretion and failure events are hard to achieve (Hancock et al., 2020). Specifically, measuring the horizontal growth of snow cornice (Vogel et al., 2012) and recording dynamic details of snow mass transport simultaneously is hard to achieve. There are few laboratory experiments on cornice formation except Naruse et al. (1985) and Naito and Kobayashi (1986). Naito and Kobayashi (1986) carried out experiments both in the wind tunnel and in the field, observing the process of snow cornice growth. They described the snow cornice formation as a process in which drifting snow particles adhere one after another at the leeward edge, in the form of a thin slab of snow elongating leewards, then the slab hangs down under its weight, depositing drifted snow particles on it. However, quantitative descriptions of this

process have not been reported. Their results show that the cornice growth under suitable conditions of the air temperature is between -20 °C to 0°C, the wind speed is between 4 m s^{-1} to 8 m s^{-1}, and fresh snow with an irregular dendritic shape. However, further quantitative analysis of experiments has not been carried out. Mott et al. (2010) have indicated that snow cornice formation is mainly through snow distribution processes driven by saltation. However, due to the lack of physical mechanism of snow cornice formation, cornice characteristic features could not be reproduced in numerical simulation of snow distribution in mountain areas (Gauer, 2001). Thus, there is still no snow cornice prediction model that could be used in avalanche prevention so far.

Therefore, wind tunnel experiments with controlled environmental conditions and quantitative descriptions of the individual cornice formation process as a pathway to improve the understanding of cornice dynamics in the field, particularly on the wind effects on cornice formation, are essential. In this work, wind tunnel experiments of snow cornice evolution on the edge of a small-scaled mountain ridge model carried out in a cold laboratory at WSL Institute for Snow and Avalanche Research (SLF) are presented. Quantitative estimations on the effect of wind conditions on snow cornice formation are presented. Section 2 presents the experimental setup in the cold laboratory and the post-processing method for cornice images. General features of the snow cornice observed in the experiment under variable wind conditions are shown in section 3. Based on this, a conceptual model evaluating the growth rates of the snow cornice based on the mass conservation method is proposed in Section 4. Its application in field observation results is discussed. Section 5 summarizes the conclusions and outlook.

2 Methods

2.1 Experimental Setup

The experiments were carried out in a cold laboratory of the SLF in Davos, Switzerland, where the room temperature can be controlled from −25 °C to 0 °C. An obround, closed-circuit wind tunnel built by Sommer et al. (2017, 2018) was used to perform the investigations. During the experiment, the room temperature of the cold laboratory was set to be −5 °C.

The schematic diagram of the experimental setup is shown in Fig. 1. The ring wind tunnel (RWT) contains two straight sections (length = 1 m, marked as S1 and S2) and two half-circle sections (outer diameter = 0.6 m, marked as H1 and H2). Its cross-section area is 0.2 m (width) × 0.5 m (height). An electric motor with rotor blades installed inside the middle of H1 creates the wind flow with a wind speed range of 0–8 m s^{-1}. A sieve is installed at S1, where the tunnel has an upward open window to supply snow particles. Sensors monitoring the air conditions are installed at the inlet of S2. The details of the sensors are listed in Table1. The ridge model in S2 with the fixed size and place is built with compacted snow each time before the experiment. The size of the ridge model was set as 0.125 m in height and with a 0.1 m flat section. The slope angle relative to the horizontal direction is 36 °. To record the growth of the cornice using shadowgraphy imaging, we placed a CMOS Camera with a spatial resolution of 2048 × 2048 pixels to zoom on the edge of the ridge. We placed a LED lamp on the opposite side for illumination.

Fresh snow particles made with a snowmaker developed at SLF (Schleef et al., 2014) were used for feeding the flow through the sieve. When using the snowmaker, the room temperature was set to −20 °C, and the water inside the snowmaker reservoir

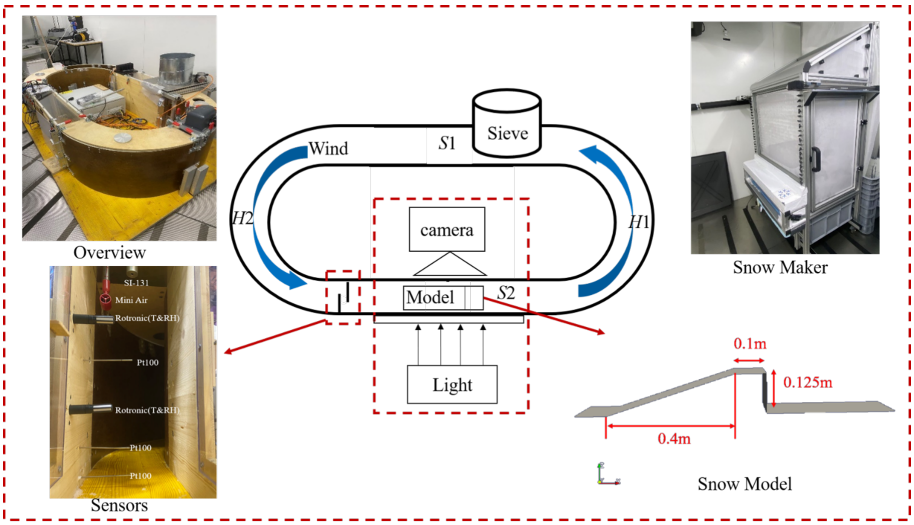

Figure 1. Schematic diagram of the closed-circuit tunnel experimental system in the cold lab. The insets are the pictures of the RWT, Snow Maker , sensors, and the snow model set up inside the RWT.

Table 1. Instruments, variables, and data acquisition interval.

Instrument	Instrument model	Variables	Time interval (s)
CMOS Camera	LP285-40.5	Images	0.02
Wind Speed Tester	Mini Air	u (m s^{-1})	0.2
Snow Temperature	Pt100	T (K)	1
Snow Surface Temperature	SI-131	T_s (K)	1
Air Temperature and RH	Rotronic	T (K) and RH (%)	1

was set to 30 °C. The obtained fresh snow is a mixture of dendritic crystals and hollow columns. The average diameter was about 300-500 μm, estimated by a grid plate and an amplifying lens. The specific surface area (SSA) was about 12-20 mm^{-1} for the snow was stored a few days up to a week (Schleef et al., 2014). A constant seeding rate is applied for all experimental tests, and the wind tunnel is cleaned up before each test. Impact threshold wind speed in the experiment is determined 1) by increasing the wind speed from zero until saltating particles can be observed; 2) by decreasing the wind speed slowly, until snow saltation is not visible anymore. The average wind speed at these two times is considered the impact threshold wind speed (Walter et al., 2014). The average impact threshold wind speed was 3.2 m s^{-1} at the height of the mini-air wind sensor. Thus, seven target wind speed conditions (from 3.0 m s^{-1} to 6.5 m s^{-1} by steps of 0.5 m s^{-1}) were set for the experiments. Once the propeller starts to rotate, the wind speed increases until it reaches the target value. The propeller angular velocity is adjusted throughout the experiment to keep the wind speed constant.

2.2 Image Processing

The CMOS camera recorded 50 images with a frequency of 10 Hz in the burst mode, and the pause between two bursts was 5 s. Thus, 50 continuous frames in 5 s as one set was obtained, which could estimate the cornice growth rate and transport mass flux instantaneously or on average. The first image, in which only the ridge model was visible without snow particles moving across, was set as a background image, as shown in Fig. 2a. For a set of 50 frames, the images were subtracted from the background image (only with ridge model) and transformed to binary format (where the grayscale value of pixels with snow is 1, and without snow is 0), as shown in Fig. 2c-e. The cornice length L (m) and cornice thickness H (m) are calculated based on the binary images (Fig. 2c-d). To avoid a wrong interpretation (as erosion or deposition) of the shape effect of bending, we used the thickness of accumulation mass on the flat as the indicator of vertical accumulation/erosion of the cornice in the following analysis.

The instantaneous cornice growth or erosion rate in thickness $h_{g/e}$ (m s^{-1}) and in length $l_{g/e}$ (m s^{-1}) are then calculated as the difference of two adjacent frames divided by the time difference between two images Δt (s):

$$h_{g/e} = \frac{\Delta H}{\Delta t} \tag{1}$$

$$l_{g/e} = \frac{\Delta L}{\Delta t} \tag{2}$$

The pure deposition rates in length l_d and in thickness h_d are calculated as the sum of the growth rate and the absolute value of erosion rate:

$$l_d = l_g + |l_e| \tag{3}$$

$$h_d = h_g + |h_e| \tag{4}$$

A window Ω with an area of 1 cm $\times$ 1 cm slightly above the snow cornice is chosen to calculate the mean mass concentration of particles in the air as shown in Fig. 2e. Ignoring the overlapping particles, we calculate the total volume of snow particles in Ω as the orthographic projection area of snow particles multiplied by its average diameter. Thus, the mass concentration ϕ_{p} (kg m^{-3}) can be estimated as:

$$\phi_{\mathrm{p}} = \frac{\rho_{\mathrm{i}} \bar{d}_{\mathrm{p}} \Sigma_{\Omega} g_j A_0}{S_0 \times p} \tag{5}$$

where ρ_{i} (kg m^{-3}) is the ice density, d_p (m) is the averaged diameter, g_j is the binary value of the j^{th} pixel in window Ω, A_0 = $\frac{7.7 \times 7.7}{2048 \times 2048}$ cm^2 is the area of a pixel, S_0 = 1 cm^2 is the area of the window Ω, p = 3.5 cm is the depth of field where particles can be detected in this width range (Crivelli et al., 2016). The transport mass flux q_p (kg m^{-2} s^{-1}) can be estimated using:

$$q_p(z) = \phi_p(z) u_p \tag{6}$$

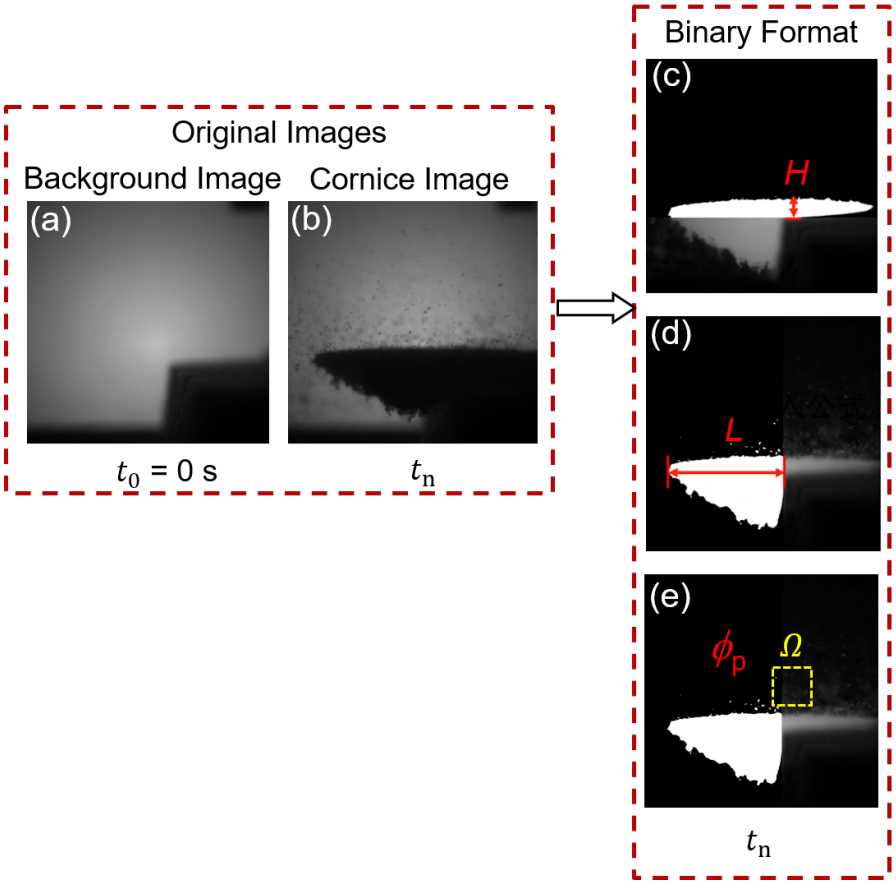

Figure 2. Post-Processing images using the grayscale method. Raw images of background (a) and cornice (b). The binary format of images with information of thickness accumulation H (c), length growth L (d), and airborne snow particles mass concentration ϕ_p captured in window Ω (e).

where $\phi_p(z)$ is the mass concentration calculated by Eq. (1), and u_p is the averaged particle velocity, which is assumed to be 10% lower than the wind speed (Nishimura et al., 2014).

$$q_p(z) = Ae^{-R_0 z} \tag{7}$$

where A and R_0 are constants that change with wind speed. The transport rate Q (kg m^{-1} s^{-1}) can be obtained by integrating the mass flux profiles over height:

$$Q = \int_0^\infty q_p(z)dz = \int_0^\infty Ae^{-R_0 z}dz = -\frac{A}{R_0}e^{-R_0 z}|_{z=0}^{z=\infty} = \frac{A}{R_0} \tag{8}$$

To quantify the exchange of snow between the mass flux and the cornice, we defined the relative mass flux collection efficiency ($\%$) as:

$$E = \frac{S_c \times \rho_i}{Q} \times 100\% \tag{9}$$

where $S_c = \frac{dA_c}{dt}$ is the growth rate of the cornice projected area A_c.

3 Results

3.1 General observations on snow cornice formation

By post-processing the high-speed camera images from the experiments, the profiles of the snow cornice are obtained as shown in Fig. 3a. The time series of the cornice length L, thickness H, and the mass concentration of airborne snow ϕ_p are then estimated as shown in Fig. 3b. Here, we use the case of wind speed u = 4 m s $^{-1}$ as an example to present the cornice growth process. As is shown in Fig. 3b, the cornice size information associated with wind speed and particle mass concentration are presented. The wind speed increased from 0 to 4 m s $^{-1}$ in about 210 s and was then kept stable during the cornice formation process. The particle mass concentration started to increase at t = 176 s (marked in black dash line: $u = u_t$) and reached a stable value at t = 250 s. The cornice started to grow when the wind speed exceeded the threshold. The growth rate was not stable at first because the initial growth of cornice is in intermittent drifting snow when the aerodynamic entrainment is still dominant in the initial stage of drifting snow (Li et al., 2018). The linear length growth stage is when the wind speed and mass concentration values arrive stable.

During cornice accretion, there are two stages for the growth of the cornice. In the first stage, a few particles stop on edge and compose a 0.011 m small and thin slab that forms leeward from the ridge model's edge. The shape profile of this slab is shown as from t_1 to t_3 in Fig. 3a. In the second stage (from t = 320 s in Fig. 3b), the cornice thickness grows simultaneously with the length. With more layers overlapping on the surface, the cornice starts slightly bending down.

When the cornice length reaches the boundary of the view, we stop seeding. Erosion first affects the thickness of the snow cornice. The downward bending continues (outlines from t_7 to t_8 in Fig. 3a and t = 430 - 440 s in Fig. 3b). During this period, aerodynamic entrainment dominates the erosion process. As is shown in Fig. 3b, the mass flux markedly decreases as the aerodynamic entrainment is inhibited by the surface morphology formed during the redistribution of the snow deposition in the RWT.

3.2 Mass flux and collection efficiency

Since the magnitude of drifting snow is critical for the vertical and horizontal cornice growth rates, the mass transport rates were calculated for the different experiments and analyzed in terms of mass exchange between the cornice and the saltation layer. The mass flux variation with height over snow cornices can be estimated by multiple windows Ω that are continuously distributed in height, as is shown in Fig. 4. The mass flux exponentially decreases with the increasing height in each wind condition, and its value increases with the wind speed, which is consistent with previous results (Takeuchi, 1980; Lehning et al., 2002; Kosugi et al., 2008; Lü et al., 2012; Crivelli et al., 2016; Melo et al., 2022).

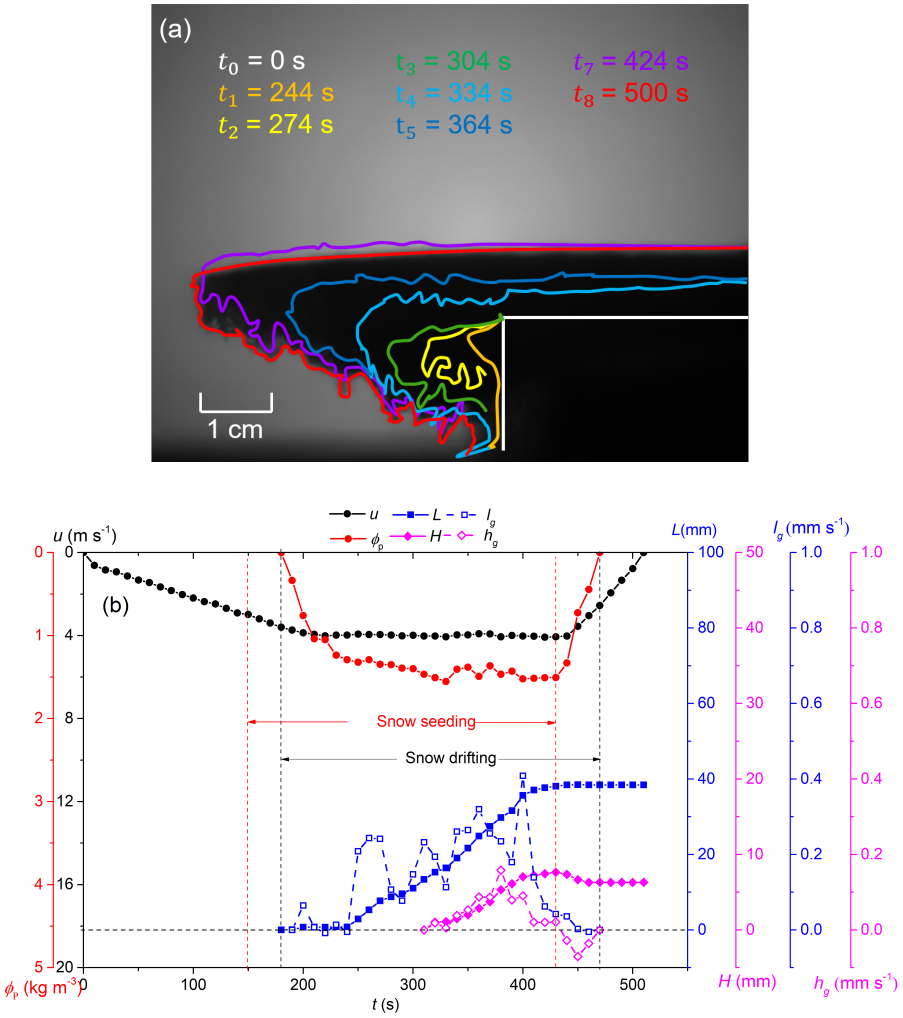

Figure 3. (a) Cornice profiles in the growth process. (b) Variation of cornice length (blue squares), thickness (pink squares), length growth rate (blue hollow squares), cornice thickness growth rate (pink hollow square), wind speed (black circles) and particle mass concentration in the air (red circles).

By fitting Eq. (7) using the estimated mass flux from the shadow images, we obtain A and R_0 for different wind speeds, as summarized in Table 2. Their fitted functions are: $A = -2092 + 1840u - 596u^2 + 84u^3 - 4u^4$ and $R_0 = -285.95 + 118.29u$. As is shown in Fig. 4, the transport mass flux profile can be described by an exponential law (Nishimura and Nemoto, 2005; Sugiura et al., 1998).

A non-dimensional wind speed $\tilde{u} = \frac{u}{u_t}$ is defined here to compare with the experimental results of Naito and Kobayashi (1986). In this definition, u_t is the threshold wind speed which can be considered as the lower limit wind speed value for cornice growth. As is shown in Fig. 5, the mass collection efficiency in both experiments decreases with the increasing wind

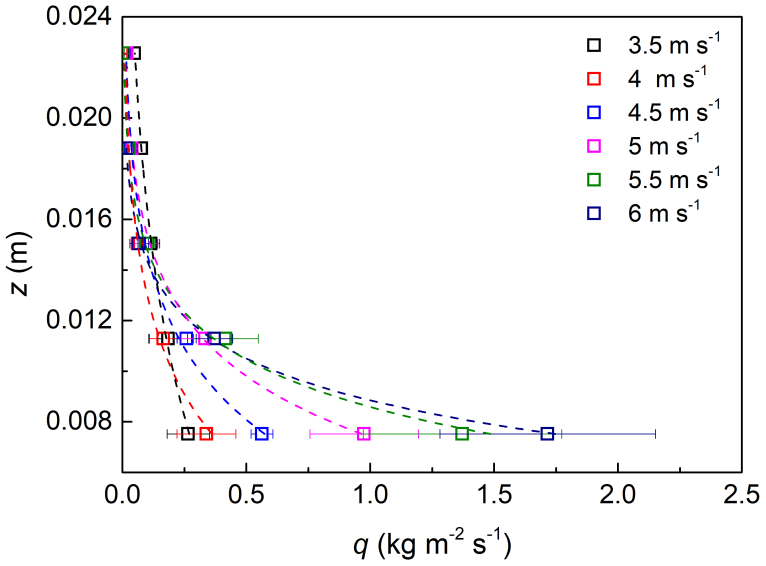

Figure 4. Mass flux variation with height under different wind conditions (3.5-6 m s^{-1}). The dashed lines are exponential fitted.

Table 2. Coefficients of A and R_0 for different wind speeds u.

Wind Speed u (m s^{-1})	***A***	$\boldsymbol{R_0}$
3.5	0.62	109.42
4	2.09	218.5
4.5	3.63	245.32
5	8.44	288.16
5.5	24.05	370.31
6	40.72	418.78

speed and the corresponding drift rate. Our experimental results are much larger than that in N&K86, which is mainly due to the different wind tunnel sizes.

170 The collection efficiency cannot directly reflect the cornice growth characteristics because it represents the proportion of snow particles passing through the edge and stopping by. This value only reflect the effective contribution of the drifting snow to the snow cornice formation under different wind conditions. Thus, to characterize the growth rate of cornice, it is necessary to analyze the absolute amount of accumulated particles as a function of time and wind speed which is introduced in the Section 3.3.

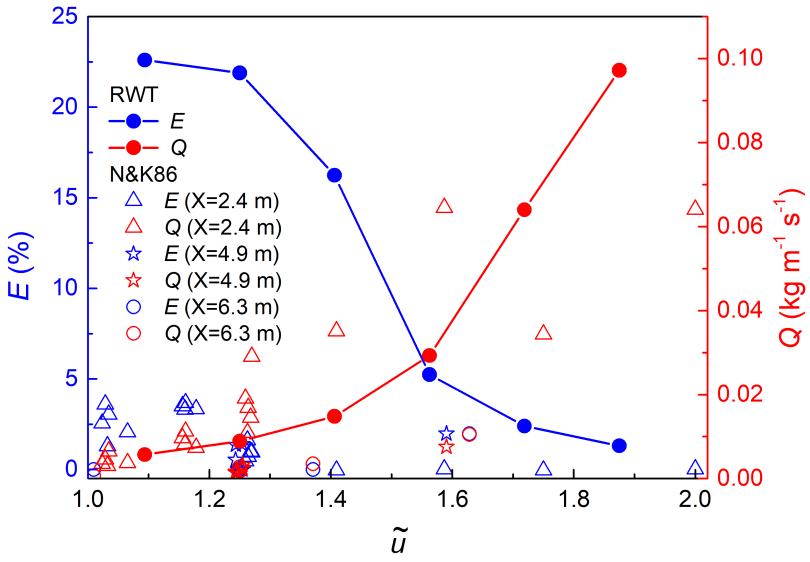

Figure 5. Collection efficiency E (in blue) and snow transport rate Q (in red) under different non-dimensional wind speeds $\tilde{u}$. X represents the distance from the snow particle feeding point to the mass collection pits where the cornice grows. Lines are for ring wind-tunnel experiments, hollow scatters are for N&K86. N&K86 represents the experiment results of Naito and Kobayashi (1986)

3.3 The suitable wind speed range for cornice formation

Cornice formation was tested with wind speeds from 3 m s^{-1} to 6.5 m s^{-1} using 0.5 m s^{-1} increments. In each wind condition, the averaged cornice growth rates in length and thickness are: $\overline{l}_g$ (m s^{-1}) and $\overline{h}_g$ (m s^{-1}) (with seeding), and erosion rates: $\overline{l}_e$ (m s^{-1}) and $\overline{h}_e$ (m s^{-1}) (without seeding) are obtained by estimating the slopes of the near-linear growth/erosion curves as is shown in the Fig. 3. Thus, the averaged pure deposition rates in length $\overline{l}_d$ and thickness $\overline{h}_d$ can be calculated by the Eq. (3-4).

As is shown in the Fig. 6, there is no cornice formation for wind speed lower than the threshold wind speed because of a missing saltation layer and snow transport. The extension line of the pure deposition rate in length tends to zero around the threshold wind speed for snow transport. Thus, we can conclude that the lower limit wind speed for cornice accretion is close to the threshold wind speed for snow transportation, which is consistent with the field study (McClung and Schaerer, 2006; Hancock et al., 2020).

The cornice length growth rate l_g reaches its maximum when the wind speed is approximately 40 % higher than the threshold wind speed. At this wind speed, the net deposition rate ($l_d - l_e$) in length reaches maximum. The erosion rates in length and thickness approximately linearly increase with the wind speed. In the cornice growing process, the length growth rate (l_g) is higher than the thickness growth rate (h_g) at all wind speed conditions. The erosion in length takes place later than in thickness, and the thickness erosion rate is always approximately 30 % higher than the length erosion rate ($l_e = 0.7h_e$).

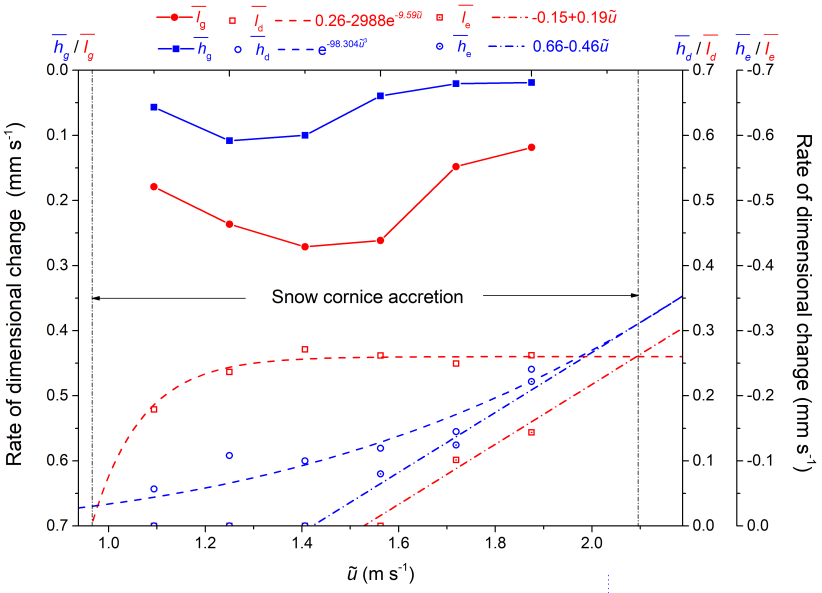

Figure 6. Growth rates, erosion rates, and the pure deposition rates in length and thickness under different wind conditions. The fitted functions are plotted in dashed lines.

The pure deposition rate in length l_d increases rapidly at first and stabilizes with the wind speed, while the erosion rate in length l_e linearly increases with the wind speed. The values of l_d and l_e arrive equivalent at the wind condition of about 6.5 m s^{-1}, at which point the mass of the pure accumulation and the erosion is balanced. Thus, the upper limit wind speed of snow cornice formation in our case is 6.5 m s^{-1} which is 2.03 times of threshold wind speed.

Overall, the cornice growth process has two stages: In the first stage, a thin slab grows and overhangs at the edge. In the second stage, cornice thickness and length both increase simultaneously. The collection efficiency, reflecting the effective contribution of the drifting snow to the snow cornice formation, cannot directly reflect the cornice growth characteristics. Instead, the pure deposition rates, the erosion rates, and the growth rates both in length and thickness were analyzed separately for all wind conditions. From the results we can conclude that in all wind conditions, the cornice starts to grow when the wind speed exceeds the threshold value, and starts to scouring when the erosion rate is over the pure deposition rate. The cornice only grows at a moderate wind speed range (1-2.03 $\tilde{u}$). The length erosion rate of the cornice is typically 30% lower relative to the thickness erosion rate. The length growth rate gets maximum at the wind speed is 40 % over the threshold. The presented framework for characterizing cornice accretion may provide a basis for future field and laboratory studies under different conditions.

4 Discussion

From the experimental results, we can conclude that cornice growth is a process of mass accumulation overgrowing the ridge under the action of wind force, accompanied by bending and erosion. The growth process of snow cornice has two stages, which can be described with a schematic shown in Fig. 7. The first stage can be assumed as a formation of the one-particle diameter-thickness snow slab composed of sticking particles at the edge. The first process is mainly determined by the spatial variation of the mass transport rate along the flow direction. The second stage can be assumed as a repeated process of length growth-thickness growth. The length growth is considered as a horizontal creeping of the newly formed snow layer, driven by the drifting snow. The thickness growth is considered as a comprehensive result of particle deposition and erosion at the edge. Thus, the second growth process is mainly dependent on the wind speed, the non-dimensional, spatial variation of mass concentration, and the particle interaction force.

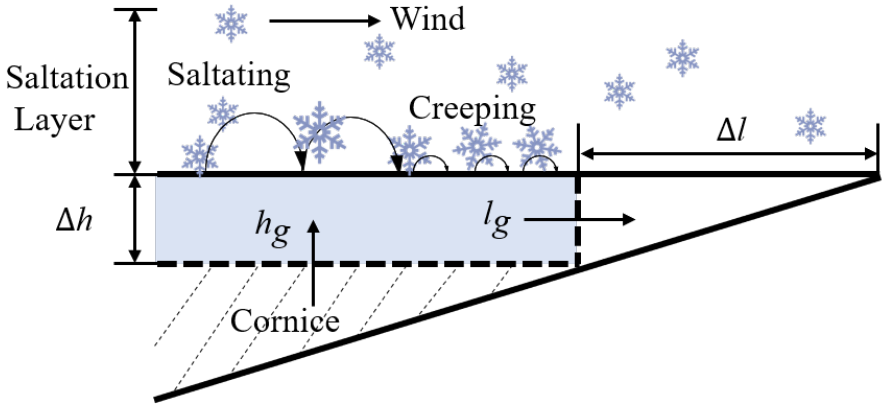

Figure 7. Schematic of snow cornice growth.

4.1 A conceptual model for cornice formation

In here, we analyze the snow cornice as the shaded area shown in the Fig. 7. Based on the law of mass conservation, the cornice thickness growth rate h_g can be calculated as the difference between the pure deposition rate in thickness h_d and the thickness erosion rate h_e. In which, the pure deposition rate in thickness $h_d = K_d \frac{\phi_p}{\rho_c}$ is calculated by the deposition rate of mass on the surface per unit time. Thus, the thickness growth rate h_g can be written as:

$$h_g = K_d \frac{\phi_p}{\rho_c} - h_e \tag{10}$$

where K_d is the deposition coefficient (m s^{-1}), $\rho_c = 147$ kg m^{-3} is the average snow density of the cornice as measured during the experiments. This value is close to the fresh snow and lower than that in the field of $\sim$ 300 kg m^{-3} (Naruse et al., 1985), which might be related to the long-term compaction of the snowpack in the field.

The cornice length growth is considered as the forward creeping of the surface layer which is driven by the drifting snow saltation. The cornice length growth rate l_g can be estimated as the difference between the pure deposition rate in length l_d and the length erosion rate l_e. In which l_d is considered as the moving distance Δl (m) of a newly formed snow layer (blue area in Fig. 7) with one particle diameter in thickness Δh (m) per unit time. The pure deposition rate in length l_d is related to the mass transport rate Q and the non-dimensional horizontal collection coefficient f_l:

$$l_g = \frac{Q f_l}{\rho_c d_p} - l_e \tag{11}$$

As we already measured the cornice thickness growth rate h_g, thickness erosion rate h_e, the cornice length growth rate l_g, length erosion rate l_e, the air mass concentration ϕ_{p}, and the mass transport rate Q, the deposition coefficient and the horizontal collection rate can be estimated as $K_d = \frac{(h_g+h_e)\rho_c}{\phi_p}$ and $f_l = \frac{(l_g+l_e)\rho_c d_p}{Q}$, which exponentially decrease with the wind speed, as shown in Fig. 8.

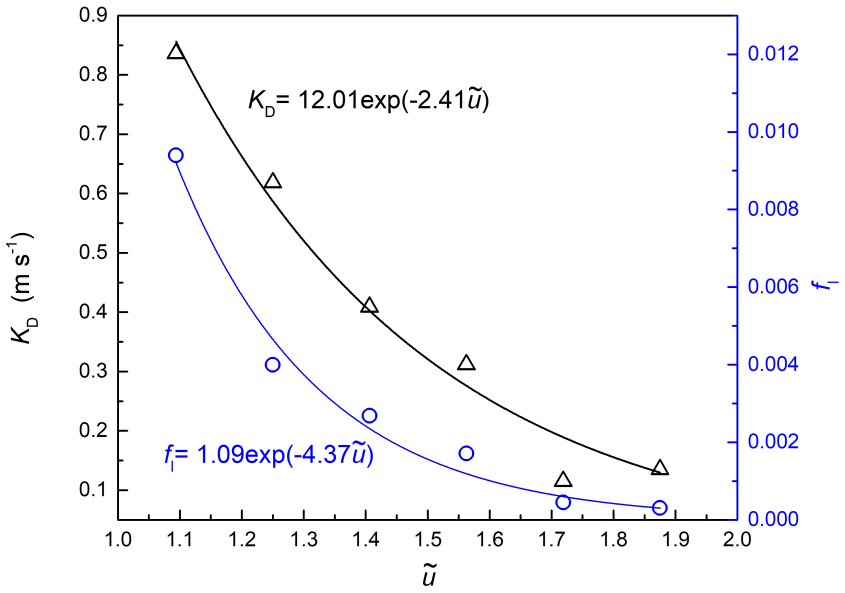

Figure 8. Deposition coefficient and the horizontal collection rate in all wind conditions. The solid lines are the fit curves.

4.2 Field predictions

To validate our conceptual model, we compare the results with two cases of the field observations.

4.2.1 Case I: Comparison of suitable wind condition with Vogel et al. (2012)

Vogel et al. (2012, abbr. as VF2012) showed cornice evolution along the ridgeline of the Gruvefjellet plateau mountain above Nybyen in the period 2008–2010. They found that the cornice accretion happened during the entire snow seasons, when the averaged hourly maximum wind speeds exceeded 12 m s^{-1}, with a minimum of at least 10 m s^{-1}.

Considering the cornice accretion always appears in snowstorms, we assume that the snow transport rate Q in the field can be expressed as the same value as its value in the saturated saltation (Sørensen, 2004):

$$Q = \frac{\rho_a}{g} u_*^3 (1 - \frac{u_{*t}^2}{u_*^2})(2.6 + 2\frac{u_{*t}}{u_*} - 2.5\frac{u_{*t}^2}{u_*^2}) \tag{12}$$

where $u_* = \frac{\kappa u_f}{ln(z_f/z_0)}$ is the friction velocity (m s^{-1}) which is calculated with the field wind speed u_f (m s^{-1}) at height z_f = 2.8 m. $\kappa = 0.4$ is the Von Kármán constant, $g = 9.8$ m s^{-2} is the gravitational acceleration and z_0 (m) is the aerodynamic roughness length. u_{*t} (m s^{-1}) is the threshold friction velocity which is calculated based on the local threshold wind speed u_t (m s^{-1}).

Then we can estimate the potential maximum erosion rate as the aerodynamic entrainment rate by:

$$M_e = m_p \cdot \eta_{ae} \rho_a (u_*^2 - u_{*t}^2) \tag{13}$$

where $m_p = \frac{1}{6}\pi {d_p}^3 \rho_i$ is the mass of a snow particle, in which the average particle diameter d_p in the field is assumed as 300 μm (Nishimura et al., 2014). $\eta_{ae} = 6 \times 10^5$ (grains N^{-1} s^{-1}) is a empirical parameter (Clifton and Lehning, 2008).

Considering the ratio of erosion rate in thickness and length l_e/h_e is about 0.7, the erosion rate in thickness can be written as $h_e = 0.7\frac{M_e}{\rho_c}$. Thus, we can rewrite the length growth rate l_g in Eq. (11) as:

$$l_g = \frac{Q f_l}{\rho_c d_p} - 0.7 M_e/\rho_c \tag{14}$$

Thus, we could infer that the length growth rate l_g is only depended on variables of the field wind speed u_f, the threshold wind speed u_t, and the roughness length z_0. To test the sensitivity of the input parameters, we choose different z_0 and u_t to estimate the length growth rate in the wind speed range of VF2012, shown as Fig. 9. The automatic weather station in Gruvefjellet is located at $\sim$ 300 m from the cornice on the plateau. The wind station is at a flat field, and the roughness length z_0 can be assumed as the measurement values on the flat snow surface. The roughness lengths z_0 vary in snow covers (Clifton et al., 2006), which typically vary over two orders of magnitude: from 10^{-5}-10^{-3} m for the fresh snow in the fields (Brock et al., 2006; König-Langlo, 1985). As is shown in the Fig. 9, the roughness length and the threshold wind speed only have effects on the magnitude of the maximum value of growth rates, while the suitable non-dimensional wind speed range remains the same. The predicted wind range for snow cornice formation is about 1 $\sim$ 2.26 times threshold wind speed, namely 10 $\sim$ 22.6 m s^{-1}, which agrees with the field observations. And the maximum value is about 30 % higher than the threshold wind speed. There is no available length growth rate data in VF2012, so we use the follow case to validate the length growth rate. For it is in the same site, we use z_0 = 10^{-4} m and u_t = 10 m s^{-1} in the following modeling.

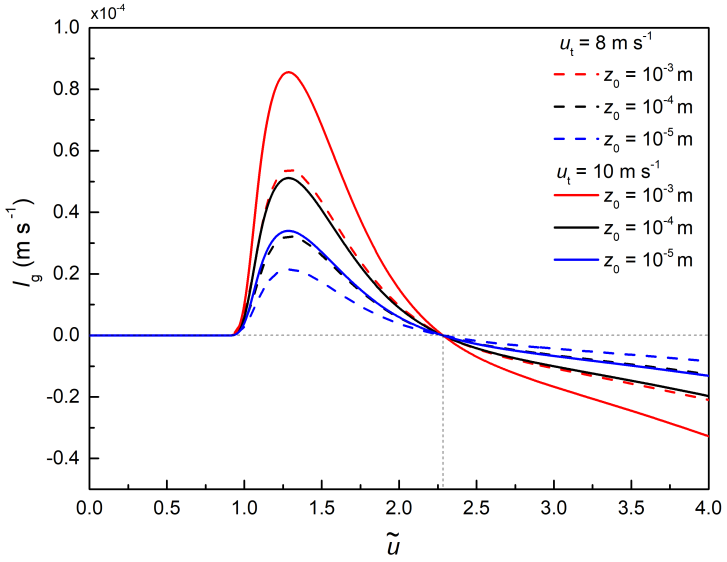

Figure 9. Estimations of cornice length growth rates in the fields.

4.2.2 Case II: Comparison of the length growth rate with Hancoko et al. (2020)

Hancock et al. (2020, abbr. HF2020) used a Riegl® Laser Measurement Systems VZ-6000 ultra-long-range terrestrial laser scanner to repeatedly scan the Gruvefjellet and Platåberget cornice systems throughout the 2016–2017 and 2017–2018 winter seasons. Three cornice accretion events were recorded with the mean length growth rate over 10 mm h^{-1}, which is about 3.9-4.7$\times$10^{-6} m s^{-1}. However, in our experiment, the average length growth rate range is 1.2-2.7$\times$10^{-4} m s^{-1}. The main reason for the discrepancies between the laboratory and the field results is due to the temporally and spatially constrained estimations of the threshold wind speeds for cornice accretion and cornice horizontal length growth rate (Vogel et al., 2012; Hancock et al., 2020). In the field, snow cornices have multiple growth periods in snowstorms that last a few hours. While in the RWT experiment, we mainly focused on a continuous growth process of a snow cornice. The fluctuating and intermittent wind in the field differs from the steady and stationary wind in the RWT, and this also causes the effective time for a cornice formation being much less than the sampling time (several hours to days). The sampling frequency is not sufficient to catch the complete accretion period for the wind in the field is gusty and intermittent. Also, in the field the cornice may partially collapse from time to time which is not recognized during the storm without any laser scanning. Thus, it is difficult to estimate the cornice length growth rate based on the daily averaged wind speed from HF2020. Here, we use the Weibull probability density function to reproduce a high resolution time series of wind speed (Fig. 10a), which can be expressed as:

$$p(u) = (\frac{k}{\lambda})(\frac{u}{\lambda})^{k-1} e^{-(\frac{u}{\lambda})^k} \quad (15)$$

in which, k is the shape factor which is normally between 1.5 to 3, depending on the wind variability. Smaller k represents more gusty wind. For example k =2 represents for the moderately gusty wind (Seguro and Lambert, 2000). In here, we assumed it as 1.7. λ is the scale factor which is calculated based on the daily averaged wind speed $\bar{u}$ and the gamma function of the inverse of the shape factor k:

$$\lambda = \frac{\bar{u}}{\Gamma(1+\frac{1}{k})} \tag{16}$$

Figure 10a shows an example of wind speed time series produced by using Eq. 15 with a mean wind speed of 5.43 m s^{-1} and time interval of 10 minutes. From the time series, we can estimated the length growth rate as:

$$l_g = \frac{1}{T}\int_0^T (\frac{Q(u)f_l(u)}{\rho_c \bar{d}_p} - 0.7E(u)/\rho_c)dt \tag{17}$$

where T (min) is the sampling time of the scanner images. The transport rate $Q(u)$, horizontal collection rate $f_l(u)$, and the mass erosion rate $E(u)$ are the functions of wind speed u in time series. To test the sensitivity of the time interval dt (min), we use values of 5 min, 10 min, 15 min, 30 min, 1 hour, 2 hour, and the estimated growth rates are shown in Fig.10b. The length growth rate trends to a stable value when the time interval is shorter than 10 minutes. Thus, in the following analysis, we used 10 minutes as the time interval of wind data sampling.

Table. 3 shows the averaged length growth rates in three cornice accretion events in HF2020. The averaged length growth rates l_g calculated from the model are comparable with that values from TLS data l_g^f (m s^{-1}) in the field (Hancock et al., 2020), which indicates that our model has the potential ability to predict the cornice accretion in the field.

Table 3. Comparison results with field observations.

Location	**Dates**	$l_g^f \times 10^{-6}$ (m s^{-1})	$l_g \times 10^{-6}$ (m s^{-1})
Plataberget	Feb17-Feb28	4.72	1.70±0.49
Gruvefjellet	Jan12-Jan21	4.72	1.47±0.74
Paltaberger	Apr25-May01	3.80	1.37±0.52

What needs to be mentioned is that to enhance the model accuracy, the values of K_d and f_l inferred in this prediction model still need re-estimation and corrections for the natural larger-scale snow cornice. These two parameters may be influenced by the local topographical features. For future accurate field predictions on the cornice on a larger scale, more field measurement data are needed, such as the snowpack thickness on the root of a cornice, the mass concentration, the threshold friction velocity, roughness length, and cornice density to calculate the proper values for K_d and f_l in the field.

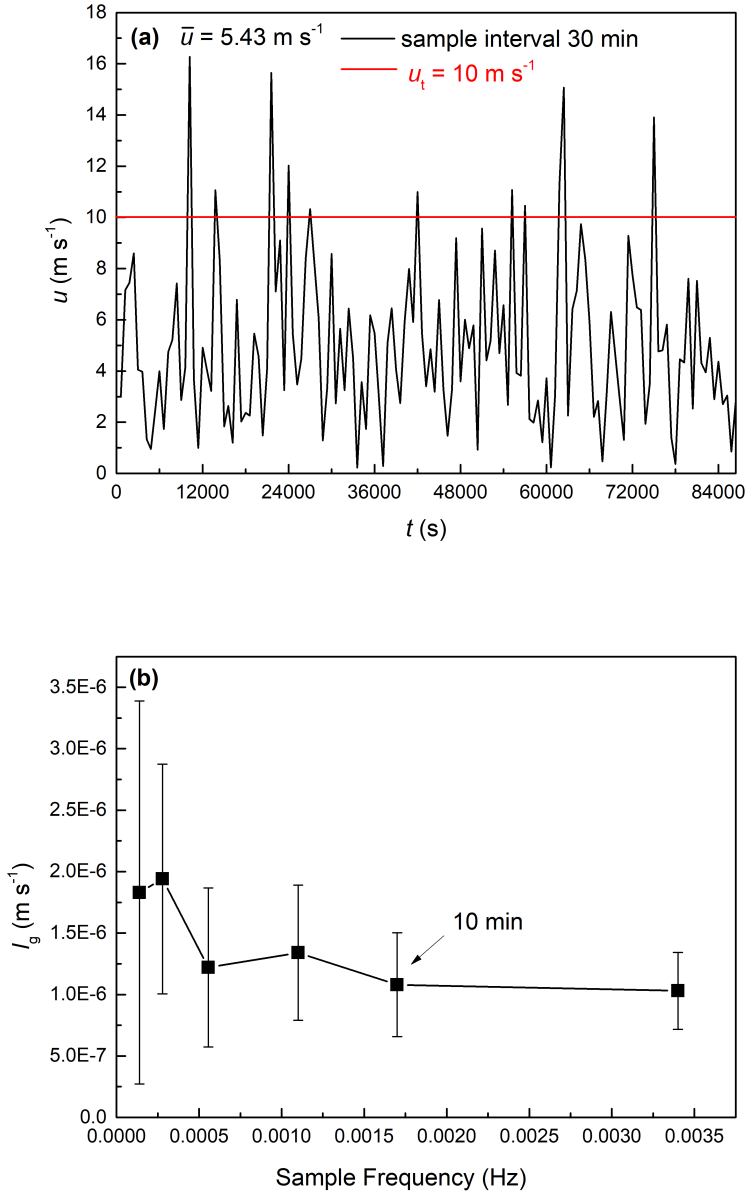

Figure 10. (a) Time series of wind speed u in one day. (b) Average length growth rates in different sample frequency.

5 Conclusions and Outlook

We carried out the RWT experiments and studied the suitable wind condition for cornice formation and growth. The results show that the snow cornices only grow at moderate wind speed with a sufficient snow mass flux over the ridge of the model. The cornice growth process has two stages. The vertical growth rate of the cornice is typically lower relative to the horizontal growth. The mass collection efficiency decreases with the increasing wind speed and the corresponding drift rate, which can not be considered the indicator for cornice growth. Instead, the growth rates of cornice in length and thickness are determined by the combined effects of mass accumulation and erosion. The lower limit of wind speed is the threshold wind speed for snow transport, and the upper limit value of wind speed is when the deposition rate and the erosion rate arrive balanced. The most favorable wind condition for cornice growth is approximately 40 $\%$ higher than the threshold wind speed for snow transport, at which the net deposition rate in length gets maximum.

Based on the experimental results, a conceptual model is proposed for interpreting the mechanism of cornice growth. The model can be applied to fields to predict the length growth rates and the suitable wind speed range, mainly determined by the parameters such as roughness length and the threshold wind speed, thus the local surface snow conditions. From the estimations at the study site of Gruvefjellet, we can conclude that the wind speed range of cornice growth is from 1-2.5 times of the threshold wind speed, which is in line with the previous observations in the fields. It is found that the most favorable wind condition for cornice growth is approximately 30 $\%$ higher than the local threshold wind speed. The discrepancies in the knowledge of the suitable wind speed range in the previous wind tunnel experiment and the field observations are mainly due to the differences in the local roughness lengths and the threshold wind speeds. In a future study, improvements of our model, such as predicting the snow cornice growth rates more accurately, still need higher frequency observation data on cornice growth and erosion and the measurements on the relevant parameters.

Author contributions. YHX, LG, and BW designed the experiments. YHX and LG conducted the experiments, performed the data analysis, and prepared the first draft. ML, ZJ, and BW reviewed and edited the paper. HN and ML organized this study, contributed to its conceptualization, discussion, and finalized the paper.

Competing interests. The authors declare that they have no conflict of interest.

Acknowledgements. The authors would like to thank Dr. Matthias Jaggi for his Snow Maker expertise. The authors appreciate Dr. Mahdi Jafari, Daniela Brito Melo, Armin Sigmund for the valuable suggestions to improve the manuscript. This work was supported by the National Natural Science Foundation of China (grant no.: 41931179 and 42006187), the Second Tibetan Plateau Scientific Expedition and Research Program (grant no.: 2019QZKK020109-2), the Fundamental Research Funds for the Central Universities (grant no.: lzujbky-2021-it29 and lzujbky-2020-pd11). And the data and code will be upload to Dryad repository after the paper is published.

References

Brock, B. W., Willis, I. C., and Sharp, M. J.: Measurement and parameterization of aerodynamic roughness length variations at Haut Glacier d'Arolla, Switzerland, Journal of Glaciology, 52, 281–297, 2006.

Clifton, A. and Lehning, M.: Improvement and validation of a snow saltation model using wind tunnel measurements, Earth Surface Processes and Landforms, 33, 2156–2173, 2008.

Clifton, A., Rüedi, J.-D., and Lehning, M.: Snow saltation threshold measurements in a drifting-snow wind tunnel, Journal of Glaciology, 52, 585–596, 2006.

Crivelli, P., Paterna, E., Horender, S., and Lehning, M.: Quantifying particle numbers and mass flux in drifting snow, Boundary-Layer Meteorology, 161, 519–542, https://doi.org/10.1007/s10546-016-0170-9, 2016.

Eckerstorfer, M. and Christiansen, H. H.: Topographical and meteorological control on snow avalanching in the Longyearbyen area, central Svalbard 2006–2009, Geomorphology, 134, 186–196, https://doi.org/10.1016/j.geomorph.2011.07.001, 2011.

Gauer, P.: Numerical modeling of blowing and drifting snow in Alpine terrain, Journal of Glaciology, 47, 97–110, 2001.

Hancock, H., Eckerstorfer, M., Prokop, A., and Hendrikx, J.: Quantifying seasonal cornice dynamics using a terrestrial laser scanner in Svalbard, Norway, Natural Hazards and Earth System Sciences, 20, 603–623, https://doi.org/10.5194/nhess-20-603-2020, 2020.

König-Langlo, G.: Roughness length of an Antarctic ice shelf, Polarforschung, 55, 27–32, 1985.

Kosugi, K., Sato, T., Nemoto, M., Mochizuki, S., Sato, A., and Prevention, D.: Vertical profiles of mass flux for different particle diameters in drifting snow over hard snow surfaces, Proceeding of the ISSW, 38, 143–152, 2008.

Lehning, M. and Fierz, C.: Assessment of snow transport in avalanche terrain, Cold Regions Science and Technology, 51, 240–252, https://doi.org/10.1016/j.coldregions.2007.05.012, 2008.

Lehning, M., Naaim, F., Naaim, M., Brabec, B., Doorschot, J., Durand, Y., Guyomarc'h, G., Michaux, J.-L., and Zimmerli, M.: Snow drift: acoustic sensors for avalanche warning and research, Natural Hazards and Earth System Sciences, 2, 121–128, https://doi.org/10.5194/nhess-2-121-2002, 2002.

Li, G., Wang, Z., and Huang, N.: A snow distribution model based on snowfall and snow drifting simulations in mountain area, Journal of Geophysical Research: Atmospheres, 123, 7193–7203, https://doi.org/10.1029/2018JD028434, 2018.

Lü, X., Huang, N., and Tong, D.: Wind tunnel experiments on natural snow drift, Science China Technological Sciences, 55, 927–938, https://doi.org/10.1007/s11431-011-4731-3, 2012.

McClung, D. and Schaerer, P. A.: The avalanche handbook, The Mountaineers Books, 2006.

Melo, D. B., Sharma, V., Comola, F., Sigmund, A., and Lehning, M.: Modeling snow saltation: the effect of grain size and interparticle cohesion, Journal of Geophysical Research: Atmospheres, 127, e2021JD035 260, 2022.

Montagnen, J., McPartland, J. T., Super, A. B., and Townes, H. W.: The Nature and control of snow cornices on the Bridger Range, Southwestern Montana, Alta Avalanche Study Center, Miscellaneous Report No. 14, 1968.

Mott, R., Schirmer, M., Bavay, M., Grünewald, T., and Lehning, M.: Understanding snow-transport processes shaping the mountain snowcover, The Cryosphere, 4, 545–559, 2010.

Naito and Kobayashi: Experimental study on the occurrence of cornice, Low Temperature Science. Physics., 44, 91–101, 1986.

Naruse, R., Nishimura, H., and Maeno, N.: Structural Characteristics of Snow Drifts and Cornices, Annals of Glaciology, 6, 287–288, 1985.

Nishimura, K. and Nemoto, M.: Blowing snow at Mizuho station, Antarctica, Philosophical Transactions of the Royal Society A: Mathematical, Physical and Engineering Sciences, 363, 1647–1662, https://doi.org/10.1098/rsta.2005.1599, 2005.

Nishimura, K., Yokoyama, C., Ito, Y., Nemoto, M., Naaim-Bouvet, F., Bellot, H., and Fujita, K.: Snow particle speeds in drifting snow, Journal of Geophysical Research: Atmospheres, 119, 9901–9913, 2014.

Schleef, S., Jaggi, M., Löwe, H., and Schneebeli, M.: An improved machine to produce nature-identical snow in the laboratory, Journal of Glaciology, 60, 94–102, https://doi.org/10.3189/2014JoG13J118, 2014.

Seguro, J. and Lambert, T.: Modern estimation of the parameters of the Weibull wind speed distribution for wind energy analysis, Journal of wind engineering and industrial aerodynamics, 85, 75–84, 2000.

Seligman, G., Seligman, G. A., and Douglas, C.: Snow structure and ski fields: being an account of snow and ice forms met with in nature, and a study on avalanches and snowcraft, Macmillan and Company, limited, 1936.

Sommer, C. G., Lehning, M., and Fierz, C.: Wind tunnel experiments: saltation is necessary for wind-packing, Journal of Glaciology, 63, 950–958, https://doi.org/10.1017/jog.2017.53, 2017.

Sommer, C. G., Lehning, M., and Fierz, C.: Wind tunnel experiments: influence of erosion and deposition on wind-packing of new snow, Frontiers in Earth Science, 6, 4, https://doi.org/10.3389/feart.2018.00004, 2018.

Sørensen, M.: On the rate of aeolian sand transport, Geomorphology, 59, 53–62, https://doi.org/10.1016/j.geomorph.2003.09.005, 2004.

Sugiura, K., Nishimura, K., Maeno, N., and Kimura, T.: Measurements of snow mass flux and transport rate at different particle diameters in drifting snow, Cold Regions Science and Technology, 27, 83–89, https://doi.org/10.1016/S0165-232X(98)00002-0, 1998.

Takeuchi, M.: Vertical profile and horizontal increase of drift-snow transport, Journal of Glaciology, 26, 481–492, https://doi.org/10.3189/S0022143000010996, 1980.

van Herwijnen, A. and Fierz, C.: Monitoring snow cornice development using time-lapse photography, in: Proceedings of the International Snow Science Workshop, pp. 865–869, 2014.

Vogel, S., Eckerstorfer, M., and Christiansen, H. H.: Cornice dynamics and meteorological control at Gruvefjellet, Central Svalbard, The Cryosphere, 6, 157–171, https://doi.org/10.5194/tc-6-157-2012, 2012.

Wahl, L., Planchon, O., and David, P.-M.: Characteristics and seasonal evolution of firns and snow cornices in the High Vosges mountains (eastern France), Erdkunde, pp. 51–67, https://doi.org/10.3112/erdkunde.2009.01.04, 2009.

Walter, B., Horender, S., Voegeli, C., and Lehning, M.: Experimental assessment of Owen's second hypothesis on surface shear stress induced by a fluid during sediment saltation, Geophysical Research Letters, 41, 6298–6305, 2014.